in Proc. IEEE GLOBECOM-2002, Taipei (Taiwan), Nov. 2002, pp. 254–258

Space-Time Synchronization Algorithms for UMTS/TDD Systems with Strong Co-Channel Interference

K. Kopsa, G. Matz, H. Artés, and F. Hlawatsch

Institute of Communications and Radio-Frequency Engineering, Vienna University of Technology
Gusshausstrasse 25/389, A-1040 Wien, Austria
phone: +43 1 58801 38983, fax: +43 1 58801 38999, email: Klaus.Kopsa@nt.tuwien.ac.at

***Abstract*— This paper presents methods for synchronization in the downlink of a UMTS/TDD system. Space-time processing based on multiple receive antennas is used to suppress potentially strong co-channel interference caused by other base stations. We develop a detection-based synchronization procedure exploiting the structure of UMTS/TDD, and we present three alternative detection algorithms. Simulation results using various propagation scenarios indicate the good performance of our synchronization methods in the presence of strong co-channel interference.**

I. Introduction

As third generation systems for mobile communications are starting to be deployed, network operators require accurate measurement tools to analyze the interference situation present. Such tools can be based on signal processing algorithms that allow to analyze the strength and origin of interfering signals. In our work, we develop algorithms that demodulate and decode the broadcast channels (BCHs) of all surrounding base stations of a UMTS/TDD network [1] and extract the cell IDs. Using this knowledge, it is possible to quantify how different base stations contribute to the total interference, thereby allowing network operators to adjust their network accordingly. An important prerequisite for demodulation of the BCHs is synchronization. In this paper, we present methods for synchronization in the downlink of a UMTS/TDD system and assess their performance.

The paper is organized as follows. In Section II, we describe the overall synchronization strategy involving a suitable detection algorithm and we show how properties of the TDD network can be exploited to improve synchronization. Three specific detection algorithms based on the generalized likelihood ratio test (GLRT) principle [2] are then presented in Section III. The performance of these algorithms is finally assessed in Section IV.

UMTS/TDD system model. In a UMTS/TDD system, each transmitted radio frame contains 15 time slots as depicted in Fig. 1 [1]. Each time slot can be allocated for uplink or downlink in a flexible manner. As shown in Fig. 2, the time slots consist of two data parts separated by a midamble and followed by a guard period. The data parts contain up to 16 data channels, each spread with a different spreading code [3]. After multiplication by the cell-specific scrambling code, the sum of the spread data channels is transmitted over a frequency-selective fading channel and received on the M-element antenna array of the mobile receiver.

Assuming K base stations and channels with P propagation paths each, the received base-band signal vector $\mathbf{x}(t)$ of size $M \times 1$ is given by

Funding by the European IST project ANTIUM and by FWF grant P15156.

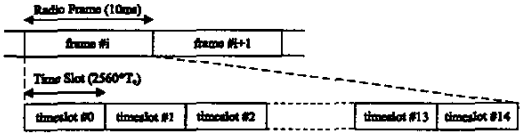

Fig. 1. Physical channel signal format [1].

Fig. 2. Time slot structure [1].

$$\mathbf{x}(t) = \sum_{i=1}^{K} \mathbf{x}_i(t) + \mathbf{n}(t) \quad \text{with} \quad \mathbf{x}_i(t) = \sum_{p=1}^{P} \mathbf{h}_{i,p}(t)\, s_i(t-\tau_{i,p}), \quad (1)$$

where $s_i(t)$ is the signal transmitted by the ith base station, $\tau_{i,p}$ and $\mathbf{h}_{i,p}(t)$ are the delay and channel weight vector, respectively, associated to the ith base station and the pth path, and $\mathbf{n}(t)$ is a noise vector. After sampling with a suitable sampling rate, we obtain the discrete-time received signal vector $\mathbf{x}(n)$.

II. UMTS/TDD Synchronization

The synchronization channel (SCH) used in UMTS/TDD is shown in Fig. 3. It consists of a primary code sequence C_p and three secondary code sequences $c_{s,j}$, each 256 chips long [3]. The three secondary synchronization codes are modulated with one QPSK symbol each that bears information on the scrambling code and midamble used by the base station and on the value of the time offset $t_{\text{offset},i}$ (cf. Fig. 3).

TDD base stations are synchronized and therefore all SCHs are transmitted in the same time slot. The different time offsets $t_{\text{offset},i}$ prevent the SCHs of different base stations from interfering. This will simplify our synchronization task because once we have obtained synchronization to the strongest base station (which can be done very reliably), we know where to look for the synchronization channels of the other, weaker base stations.

The synchronization procedure proposed here uses a detection statistic $c(n)$ that is a function of the time index n. This function is calculated from the received signal vector $\mathbf{x}(n)$ and a reference sequence $d(n)$ (to be explained presently) by means of one of the space-time algorithms that will be presented in Section III. The peaks of $c(n)$ indicate the potential presence of a synchronization code corresponding to a base station.

0-7803-7632-3/02/$17.00 ©2002 IEEE

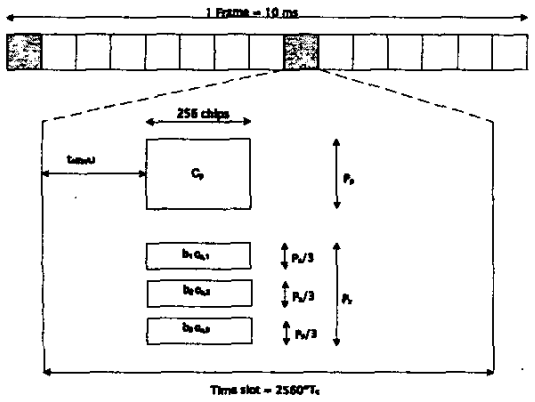

Fig. 3. Structure of the synchronization channel [1].

For primary synchronization, the reference sequence $d(n)$ is the primary synchronization code of length N. The result of primary synchronization is the temporal position of the primary synchronization code. For secondary synchronization, $d(n)$ is the sum of the primary synchronization code and three weighted secondary synchronization codes. Since there exist 64 possible combinations of weighted secondary synchronization codes, we try all corresponding $d(n)$ and take the one yielding the largest value of $c(n)$ as the result of secondary synchronization. Besides knowledge of the code group, this yields the time offset $t_{\text{offset},i}$ and with it the position of the slot border.

Synchronization to the strongest base station. Primary and secondary synchronization to the strongest base station are performed by taking the position of the highest peak in $c(n)$ as synchronization timing. The result is quite reliable because the signal-to-noise-and-interference ratio (SNIR) of the strongest base station is high. However, because the result of synchronization to the strongest base station will heavily influence the synchronization to the weaker base stations, we verify its correctness.

For this verification, we use the midamble sequence of the strongest base station as the reference sequence $d(n)$. We verify the presence of the midamble sequence at the expected location by checking if the peak of the detection statistic $c(n)$ obtained with the spatial detector (to be described in Subsection III-A) is above a certain threshold. In the negative case, we repeat secondary synchronization and midamble verification at the position of the second strongest peak of $c(n)$.

Synchronization to the weaker base stations. After verifying the synchronization to the strongest base station, we perform synchronization to the weaker base stations. For this, we exploit the fact that TDD networks are synchronized, i.e., the slot borders of all base station signals are temporally aligned.

The 32 possible time offsets $t_{\text{offset},i}$ of the synchronization codes differ by multiples of 48 chips. Since base stations in adjacent cells never use the same time offset, we know where we can expect to find the synchronization codes of weaker base stations. Because of path-length depending time delay differences,

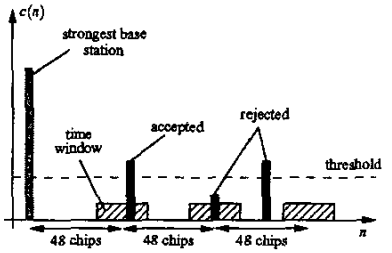

Fig. 4. Synchronization to weaker base stations using time windows.

we search for the synchronization codes in a certain time window around the expected locations, as shown in Fig. 4. The size of this window depends on the cell size and the expected maximal time delay differences. For synchronization to a weaker base station, we accept a peak of $c(n)$ only if it *both* exceeds a certain threshold and is located within one of our time windows (see Fig. 4).

It is seen that the overall synchronization procedure employs two types of thresholds, one for checking the midamble of the strongest base station and the other for primary synchronization to the weaker base stations. The choice of these thresholds is quite delicate since it corresponds to a tradeoff of detection probability against false alarm probability.

III. Space-Time Synchronization Algorithms

As explained in the previous section, the synchronization procedure employs a detection statistic $c(n)$ whose peaks indicate the potential presence and temporal location of base stations' SCHs. We now present three specific detection statistics that are based on the generalized likelihood ratio test (GLRT) principle [2].

A. Spatial Detector

The first detector [4, 5] uses the simplifying assumption of a one-tap channel described by a single $M \times 1$ vector $\mathbf{h}$. Detecting the presence of the primary synchronization code at time n can be formulated as the following hypothesis testing problem:

- Hypothesis H_0 (absence of synchronization code):

$$\mathbf{x}(n+k) = \mathbf{w}(n+k), \quad \text{for } k = 0,\ldots,N-1;$$

- Hypothesis H_1 (presence of synchronization code):

$$\mathbf{x}(n+k) = \mathbf{h}\,d(k) + \mathbf{w}(n+k), \quad \text{for } k = 0,\ldots,N-1.$$

Here, $d(k)$ is the reference sequence of length N and $\mathbf{w}(n)$ summarizes all interference from other base stations and noise. We assume that $\mathbf{w}(n)$ is Gaussian and spatially correlated with covariance matrix $\mathbf{R}$ but temporally white. Since $\mathbf{R}$ and $\mathbf{h}$ are unknown, we have to solve a composite hypothesis testing problem. In the GLRT approach we replace the unknown quantities by their conditional maximum-likelihood (ML) estimates and obtain the generalized likelihood ratio of the two hypotheses at time n as

$$L(n) = \frac{(\det \hat{\mathbf{R}}_0)^N \exp\{-Q_1(\mathbf{x})\}}{(\det \hat{\mathbf{R}}_1)^N \exp\{-Q_0(\mathbf{x})\}}, \tag{2}$$

with

$$Q_0(\mathbf{x}) \triangleq \sum_{k=0}^{N-1} \mathbf{x}(n+k)^H \hat{\mathbf{R}}_0^{-1} \mathbf{x}(n+k),$$

$$Q_1(\mathbf{x}) \triangleq \sum_{k=0}^{N-1} \left[\mathbf{x}(n+k) - \hat{\mathbf{h}}\, d(k)\right]^H \hat{\mathbf{R}}_1^{-1} \left[\mathbf{x}(n+k) - \hat{\mathbf{h}}\, d(k)\right].$$

Here, $\hat{\mathbf{R}}_0$ and $\hat{\mathbf{R}}_1$ are the conditional ML estimates of $\mathbf{R}$ under hypothesis H_0 and H_1, respectively, and $\hat{\mathbf{h}}$ is the ML estimate of $\mathbf{h}$. These estimates can be shown to be given by

$$\hat{\mathbf{R}}_0 = \hat{\mathbf{R}}_{\mathbf{xx}}(n),$$

$$\hat{\mathbf{R}}_1 = \hat{\mathbf{R}}_{\mathbf{xx}}(n) - \frac{N}{\|d\|^2} \hat{\mathbf{r}}_{\mathbf{x}d}(n) \hat{\mathbf{r}}_{\mathbf{x}d}^H(n),$$

$$\hat{\mathbf{h}} = \frac{N}{\|d\|^2} \hat{\mathbf{r}}_{\mathbf{x}d}(n),$$

where $\|d\|^2 = \sum_{k=0}^{N-1} |d(k)|^2$ and

$$\hat{\mathbf{R}}_{\mathbf{xx}}(n) = \frac{1}{N} \sum_{k=0}^{N-1} \mathbf{x}(n+k)\, \mathbf{x}^H(n+k), \tag{3}$$

$$\hat{\mathbf{r}}_{\mathbf{x}d}(n) = \frac{1}{N} \sum_{k=0}^{N-1} \mathbf{x}(n+k)\, d^*(k). \tag{4}$$

After some calculations, the (logarithm of the) generalized likelihood ratio in (2) is obtained as [5]

$$c(n) = \frac{1}{\|d\|^2} \hat{\mathbf{r}}_{\mathbf{x}d}^H(n) \hat{\mathbf{R}}_{\mathbf{xx}}^{-1}(n) \hat{\mathbf{r}}_{\mathbf{x}d}(n). \tag{5}$$

Note that $c(n)$ depends on the part of the received signal $\mathbf{x}(n)$ that is located within the interval $[n, n+N-1]$.

B. Heuristic Space-Time Detector

The spatial detector (5) used the simplifying assumption of a one-tap channel (i.e., no multipath propagation). A simple *ad hoc* method for taking into account the temporal interference caused by multipath propagation (cf. (1)) is based on stacking successive samples of the received signal vector $\mathbf{x}(n)$ into the vector

$$\tilde{\mathbf{x}}(n) \triangleq \left[\mathbf{x}^T(n)\ \mathbf{x}^T(n+1) \cdots \mathbf{x}^T(n+T_0-1)\right]^T,$$

where T_0 is the length of the temporal window considered. Formally substituting $\tilde{\mathbf{x}}(n)$ for $\mathbf{x}(n)$ in (5) then yields the detection statistic

$$c(n) = \frac{1}{\|d\|^2} \hat{\mathbf{r}}_{\tilde{\mathbf{x}}d}^H(n) \hat{\mathbf{R}}_{\tilde{\mathbf{x}}\tilde{\mathbf{x}}}^{-1}(n) \hat{\mathbf{r}}_{\tilde{\mathbf{x}}d}(n),$$

where $\hat{\mathbf{R}}_{\tilde{\mathbf{x}}\tilde{\mathbf{x}}}(n)$ and $\hat{\mathbf{r}}_{\tilde{\mathbf{x}}d}(n)$ are given by (3) and (4) with $\mathbf{x}(n)$ replaced by $\tilde{\mathbf{x}}(n)$. This detection statistic is "heuristic" as it does not correspond to a GLRT with respect to the stacked vector $\tilde{\mathbf{x}}(n)$.

C. Dispersive-Channel Detector

A GLRT-based method that takes multipath propagation into account can be obtained by explicitly including a time-dispersive channel of length L in the data model. Thus, under hypothesis H_1,

$$\mathbf{x}(n+k) = \sum_{k'=0}^{L-1} \mathbf{h}(k')\, d(k-k') + \mathbf{w}(n+k), \quad \text{for } k = 0, \ldots, N-1$$

(note that $d(k) = 0$ for $k < 0$). The hypotheses can be written as [6]

$$H_0 : \tilde{\mathbf{x}}(n) = \tilde{\mathbf{w}}(n) \quad \text{vs.} \quad H_1 : \tilde{\mathbf{x}}(n) = \mathbf{D}\tilde{\mathbf{h}} + \tilde{\mathbf{w}}(n),$$

with the $MN \times 1$ stacked data and interference vectors

$$\tilde{\mathbf{x}}(n) \triangleq \left[\mathbf{x}^T(n)\ \mathbf{x}^T(n+1) \cdots \mathbf{x}^T(n+N-1)\right]^T$$

$$\tilde{\mathbf{w}}(n) \triangleq \left[\mathbf{w}^T(n)\ \mathbf{w}^T(n+1) \cdots \mathbf{w}^T(n+N-1)\right]^T$$

(recall that N is the length of the reference sequence $d(k)$), the $ML \times 1$ stacked channel impulse response vector

$$\tilde{\mathbf{h}} \triangleq \left[\mathbf{h}^T(0)\ \mathbf{h}^T(1) \cdots \mathbf{h}^T(L-1)\right]^T,$$

and the $MN \times ML$ stacked code matrix

$$\mathbf{D} \triangleq \begin{bmatrix} d(0)\mathbf{I}_M & \mathbf{0} & \cdots & \mathbf{0} \\ d(1)\mathbf{I}_M & d(0)\mathbf{I}_M & \cdots & \mathbf{0} \\ \vdots & \vdots & \ddots & \vdots \\ d(L-1)\mathbf{I}_M & d(L-2)\mathbf{I}_M & \cdots & d(0)\mathbf{I}_M \\ d(L)\mathbf{I}_M & d(L-1)\mathbf{I}_M & \cdots & d(1)\mathbf{I}_M \\ \vdots & \vdots & & \vdots \\ d(N-1)\mathbf{I}_M & d(N-2)\mathbf{I}_M & \cdots & d(N-L)\mathbf{I}_M \end{bmatrix}$$

(we assume $L \leq N$). Again, not knowing $\tilde{\mathbf{R}}$ (the covariance matrix of the stacked interference $\tilde{\mathbf{w}}(n)$) and $\tilde{\mathbf{h}}$, we substitute the conditional ML estimates to obtain the generalized likelihood ratio

$$L(n) = \frac{\det \hat{\tilde{\mathbf{R}}}_0 \exp\left\{-\tilde{Q}_1(\mathbf{x})\right\}}{\det \hat{\tilde{\mathbf{R}}}_1 \exp\left\{-\tilde{Q}_0(\mathbf{x})\right\}}, \tag{6}$$

with

$$\tilde{Q}_0(\mathbf{x}) = \tilde{\mathbf{x}}^H(n) \hat{\tilde{\mathbf{R}}}_0^{-1} \tilde{\mathbf{x}}(n),$$

$$\tilde{Q}_1(\mathbf{x}) = \left[\tilde{\mathbf{x}}(n) - \mathbf{D}\hat{\tilde{\mathbf{h}}}\right]^H \hat{\tilde{\mathbf{R}}}_1^{-1} \left[\tilde{\mathbf{x}}(n) - \mathbf{D}\hat{\tilde{\mathbf{h}}}\right].$$

Here $\hat{\tilde{\mathbf{R}}}_0$ and $\hat{\tilde{\mathbf{R}}}_1$ are the conditional ML estimates of $\tilde{\mathbf{R}}$ under hypothesis H_0 and H_1, respectively. Furthermore, $\hat{\tilde{\mathbf{h}}}$ is the ML channel estimate that is given by

$$\hat{\tilde{\mathbf{h}}} = (\mathbf{D}^H\mathbf{D})^{-1}\mathbf{D}^H\tilde{\mathbf{x}}(n).$$

Unfortunately, closed-form expressions of $\hat{\tilde{\mathbf{R}}}_0$ and $\hat{\tilde{\mathbf{R}}}_1$ do not appear to be available. To simplify, we assume that the interference $\mathbf{w}(n)$ (not $\tilde{\mathbf{w}}(n)$!) is temporally white. The matrix $\tilde{\mathbf{R}}$ is then block-diagonal with identical $M \times M$ diagonal elements $\mathbf{R}$ (cf. Subsection III-A). Furthermore, we will use the structured conditional least-squares estimates [7] of $\tilde{\mathbf{R}}$, to be denoted as $\hat{\tilde{\mathbf{R}}}_{\mathrm{LS},0}$ and $\hat{\tilde{\mathbf{R}}}_{\mathrm{LS},1}$, instead of the structured conditional ML estimates $\hat{\tilde{\mathbf{R}}}_0$ and $\hat{\tilde{\mathbf{R}}}_1$. It can be shown that this corresponds to estimating the diagonal block $\mathbf{R}$ as follows. Under H_0,

$$\hat{\mathbf{R}}_{\mathrm{LS},0}(n) = \frac{1}{N} \sum_{k=0}^{N-1} \mathbf{x}(n+k)\, \mathbf{x}^H(n+k),$$

which is seen to equal $\hat{\mathbf{R}}_0 = \hat{\mathbf{R}}_{\mathbf{xx}}(n)$ in (3). Under H_1,

$$\hat{\mathbf{R}}_{\mathrm{LS},1}(n) = \frac{1}{N}\sum_{k=0}^{N-1} \mathbf{y}(n+k)\,\mathbf{y}^H(n+k),$$

where the $M \times 1$ vectors $\mathbf{y}(n+k)$ are the blocks of the $MN \times 1$ stacked vector $\tilde{\mathbf{y}}(n) \triangleq [\mathbf{y}^T(n)\ \ \mathbf{y}^T(n+1) \cdots \mathbf{y}^T(n+N-1)]^T$ that is given by

$$\tilde{\mathbf{y}}(n) = \left[\mathbf{I}_{MN} - \mathbf{D}(\mathbf{D}^H\mathbf{D})^{-1}\mathbf{D}^H\right]\tilde{\mathbf{x}}(n).$$

The resulting modified generalized likelihood ratio (i.e., $L(n)$ in (6) using $\hat{\mathbf{R}}_{\mathrm{LS},0}(n)$ and $\hat{\mathbf{R}}_{\mathrm{LS},1}(n)$) then yields the detection statistic

$$c(n) = \frac{\det \hat{\mathbf{R}}_{\mathrm{LS},0}(n)}{\det \hat{\mathbf{R}}_{\mathrm{LS},1}(n)}.$$

IV. Simulation Results

For our simulations, we used Clarke's channel model [8] according to which the channel weight vector associated to the ith base station and the pth path (cf. (1)) is given as

$$\mathbf{h}_{i,p}(t) = \sum_{l=1}^{N_p^{(i)}} c_{p,l}^{(i)} \exp\left(\mathrm{j}\left[\frac{2\pi v}{\lambda\cos(\theta_{p,l}^{(i)} - \gamma)}t + \varphi_{p,l}^{(i)}\right]\right)\mathbf{s}_{p,l}^{(i)}.$$

Here, $N_p^{(i)}$ is the number of subpaths associated to the pth propagation path; $c_{p,l}^{(i)}$, $\theta_{p,l}^{(i)}$, $\varphi_{p,l}^{(i)}$, and $\mathbf{s}_{p,l}^{(i)}$ are respectively the amplitude factor, azimuth, phase, and steering vector of the lth subpath of the pth path; v is the speed of the mobile; γ is the angle between the mobile's motion and North; and λ is the wavelength. The relevant parameters were chosen such that a Rayleigh fading channel was obtained.

The signal received from the nearest base station is corrupted by interference from the cells adjacent to the cell in which the mobile station is located. In our simulations, we considered two different propagation environments, called "outdoor" and "indoor" in what follows, that differ by their cell radius and channel parameters. For each environment, we defined two scenarios as illustrated in Fig. 5. In outdoor scenario 1, the receiver is located within the inner cell of a grid of 8 hexagonal cells. We will thus encounter one dominant base station signal and 7 weaker base station signals. In outdoor scenario 2, the receiver is located at the border of 3 cells, so that there impinge 3 equally strong base station signals and 6 weaker base station signals. Indoor scenario 1 has the same cell layout, but not the same cell radius, as outdoor scenario 1. For indoor scenario 2, cells 1 and 2 are located above and below the other cells, respectively (because the indoor environment corresponds to buildings with several floors), which again leads to 3 equally strong base station signals.

In addition, we used two different channel parameter settings called A and B for each environment and scenario. For the outdoor environment, channel A has 3 multipath components (3 taps) with a maximum delay of only 2 chips, whereas channel B has 8 taps with a maximum delay of 15 chips. For the indoor environment, channel A still has 3 taps with a maximum delay of 2 chips, but channel B now has 4 taps with a maximum delay of 3 chips.

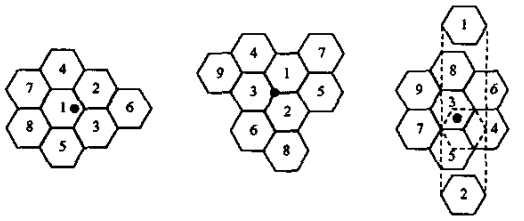

Fig. 5. Simulation scenarios. The bullet • indicates the receiver position.

False alarm probability vs. threshold. As mentioned in Section II, the choice of the thresholds to which the peaks of the detection statistic $c(n)$ are compared is critical since these thresholds determine the detection and false alarm probabilities. Fig. 6 (see top of next page) shows the false alarm probabilities vs. the threshold for the three different detector algorithms from Section III. These results were obtained for the outdoor environment with scenario 1 and channel A, using averaging of the detection statistic $c(n)$ over several successive frames. It is seen that this averaging increases the slope of the curves and thus eases the choice of the threshold.

Synchronization results. Tables I and II show the percentage of successful synchronization events for the two different outdoor scenarios with channel parameter settings A and B vs. the SNIRs of the various base stations. Tables III and IV show analogous results for the indoor environment. In both cases, the velocity of the mobile was set to 5 km/h, which is realistic for the measurement application considered. The results were obtained by averaging over 4 frames.

These simulation results show that the spatial algorithm performs quite well, especially for channel A. Reliable synchronization can be achieved down to an SNIR of about −15 dB for channel A and down to about −10 dB for channel B. For channel B, because of its larger delay, the space-time methods show superior performance; this is especially true for the outdoor environment. For the outdoor environment, synchronization using the heuristic space-time algorithm is possible down to about −18 dB for channel A and about −15 dB for channel B. For the indoor en-

TABLE I

Percentage of successful synchronization events for the outdoor environment, scenario 1. The SNIRs of the base stations are shown in the first column. The columns labeled "Spatial," "HST," and "DC" show the results obtained with the spatial detector from Subsection III-A, the heuristic space-time detector from Subsection III-B, and the dispersive-channel detector from Subsection III-C, respectively.

Algorithm	Spatial		HST		DC	
Channel	A	B	A	B	A	B
Station 1: −1 dB	100	98	100	99	100	100
Station 2: −11 dB	100	92	100	99	100	96
Station 3: −11 dB	100	90	100	99	100	95
Station 4: −18 dB	91	20	97	64	86	27
Station 5: −18 dB	94	26	97	61	87	19
Station 6: −22 dB	59	2	61	12	53	2
Station 7: −22 dB	59	3	67	23	57	13
Station 8: −22 dB	78	6	78	33	68	6

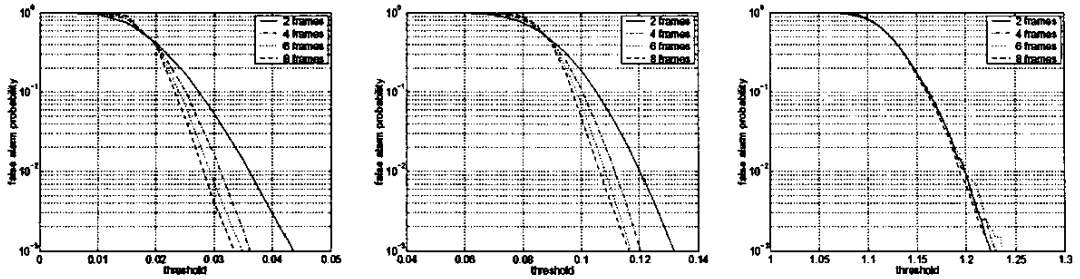

(a) (b) (c)

Fig. 6. False alarm probability vs. threshold (obtained for the outdoor environment, scenario 1, channel A) using (a) the spatial detector, (b) the heuristic space-time detector, and (c) the dispersive-channel detector. The detection statistic $c(n)$ was averaged over 2, 4, 6, or 8 frames.

TABLE II

Percentage of successful synchronization events for the outdoor environment, scenario 2.

Algorithm	Spatial		HST		DC	
Channel	A	B	A	B	A	B
Station 1: −5.1 dB	100	61	100	99	100	100
Station 2: −5.1 dB	100	56	100	99	100	100
Station 3: −5.1 dB	100	56	100	99	100	100
Station 4: −17.1 dB	84	10	89	41	86	25
Station 5: −17.1 dB	84	12	88	52	82	32
Station 6: −17.1 dB	86	18	85	65	84	38
Station 7: −22.1 dB	45	0	47	8	43	5
Station 8: −22.1 dB	54	1	41	12	40	6
Station 9: −22.1 dB	41	2	42	5	34	0

TABLE III

Percentage of successful synchronization events for the indoor environment, scenario 1.

Algorithm	Spatial		HST		DC	
Channel	A	B	A	B	A	B
Station 1: −1.7 dB	100	100	100	100	100	100
Station 2: −9.7 dB	98	99	100	100	99	96
Station 3: −9.7 dB	100	99	100	100	100	99
Station 4: −14.7 dB	87	78	96	96	87	82
Station 5: −14.7 dB	89	89	96	97	88	83
Station 6: −17.7 dB	66	60	77	87	64	55
Station 7: −17.7 dB	65	65	85	87	77	67
Station 8: −17.7 dB	77	68	90	93	73	69

TABLE IV

Percentage of successful synchronization events for the indoor environment, scenario 2.

Algorithm	Spatial		HST		DC	
Channel	A	B	A	B	A	B
Station 1: −6.1 dB	100	89	100	100	100	100
Station 2: −6.1 dB	100	88	100	100	100	100
Station 3: −6.1 dB	100	88	100	100	100	100
Station 4: −10.1 dB	99	87	99	100	98	97
Station 5: −10.1 dB	99	88	100	100	99	97
Station 6: −17.1 dB	59	34	68	70	55	37
Station 7: −17.1 dB	58	39	76	76	66	57
Station 8: −20.1 dB	39	16	53	41	32	19
Station 9: −20.1 dB	36	18	41	44	37	20

vironment, the performance of the heuristic space-time algorithm for channel B is even slightly superior to that for channel A.

The dispersive-channel algorithm falls short of the heuristic space-time algorithm and for channel A even of the spatial algorithm. The dispersive-channel algorithm is superior to the spatial algorithm only for channel B, but also there the heuristic space-time algorithm performs best. One reason may be that the comparatively large number of parameters used by the dispersive-channel algorithm cannot be estimated with sufficient accuracy.

V. Conclusion

We presented space-time synchronization methods for the downlink of a UMTS/TDD system with potentially strong co-channel interference. Our methods are based on a generalized likelihood ratio test approach and on the fact that TDD networks are synchronized. Simulation results showed that reliable synchronization down to an SNIR of about -18dB is possible for realistic propagation and interference scenarios. Our methods are thus able to resolve interference situations that can seriously affect mobile reception. We note that channel estimation algorithms for the UMTS/TDD system considered will be presented in [9].

Acknowledgments

The authors would like to thank P. Loubaton and J.-M. Chaufray (Université de Marne-la-Vallée) for numerous helpful suggestions and discussions.

References

[1] 3GPP TS 25.221, "Physical channels and mapping of transport channels onto physical channels (TDD)," v. 4.0.0 (www.3gpp.org), March 2001.

[2] Stephen M. Kay, *Fundamentals of Statistical Signal Processing: Detection Theory*, Prentice Hall, Upper Saddle River (NJ), 1998.

[3] 3GPP TS 25.223, "Spreading and modulation (TDD)," v. 4.0.0 (www.3gpp.org), March 2001.

[4] L. E. Brennan and I. S. Reed, "An adaptive array signal processing algorithm for communications," *IEEE Trans. Aerospace and Electronic Systems*, vol. 18, no. 1, pp. 124–130, Jan. 1982.

[5] D. M. Dlugos and R. A. Scholtz, "Acquisition of spread spectrum signals by an adaptive array," *IEEE Trans. Acoust., Speech, Signal Processing*, vol. 37, no. 8, pp. 1253–1270, Aug. 1989.

[6] D. M. Dlugos, *Acquisition of spread spectrum signals by an adaptive array*, Ph.D. thesis, University of Southern California, March 1986.

[7] Louis L. Scharf, *Statistical Signal Processing*, Addison Wesley, Reading (MA), 1991.

[8] R. H. Clarke, "A statistical theory of radiomobile reception," *Bell Syst. Tech. J.*, vol. 47, pp. 957–1000, 1968.

[9] K. Kopsa, H. Artés, G. Matz, and F. Hlawatsch, "Space-time algorithms for multiuser channel estimation in the downlink of UMTS/TDD," submitted to IEEE ICC-2003, Anchorage, AK, May 2003.